

ON KINETIC SLOW MODES, FLUID SLOW MODES, AND PRESSURE-BALANCED STRUCTURES IN THE SOLAR WIND

DANIEL VERSCHAREN¹, CHRISTOPHER H. K. CHEN², AND ROBERT T. WICKS³

¹Space Science Center, University of New Hampshire, Durham, NH 03824, USA; daniel.verscharen@unh.edu

²Department of Physics, Imperial College London, London SW7 2AZ, UK; christopher.chen@imperial.ac.uk

³Mullard Space Science Laboratory, University College London, London WC1E 6BT, UK; r.wicks@ucl.ac.uk

Draft version December 3, 2024

ABSTRACT

Observations in the solar wind suggest that the compressive component of inertial-range solar-wind turbulence is dominated by slow modes. The low collisionality of the solar wind allows for non-thermal features to survive, which suggests the requirement of a kinetic plasma description. The least-damped kinetic slow mode is associated with the ion-acoustic (IA) wave and a non-propagating (NP) mode. We derive analytical expressions for the IA-wave dispersion relation in an anisotropic plasma in the framework of gyrokinetics and then compare them to fully-kinetic numerical calculations, results from two-fluid theory, and MHD. This comparison shows major discrepancies in the predicted wave phase speeds from MHD and kinetic theory at moderate to high β . MHD and kinetic theory also dictate that all plasma normal modes exhibit a unique signature in terms of their polarization. We quantify the relative amplitude of fluctuations in the three lowest particle velocity moments associated with IA and NP modes in the gyrokinetic limit and compare these predictions with MHD results and in-situ observations of the solar-wind turbulence. The agreement between the observations of the wave polarization and our MHD predictions is better than the kinetic predictions, suggesting that the plasma behaves more like a fluid in the solar wind than expected.

Keywords: plasmas – solar wind – turbulence – waves

1. INTRODUCTION

According to the magnetohydrodynamic (MHD) approximation, a collisional plasma supports four types of linear modes: the Alfvén wave, the fast-magnetosonic wave, the slow-magnetosonic wave, and the entropy mode. While the Alfvén wave is non-compressive, the two magnetosonic waves exhibit changes in the density $\delta\rho$ and the magnetic-field strength $\delta|\mathbf{B}|$, which are positively correlated in the case of the fast wave and anti-correlated in the case of the slow wave. According to the more generally valid kinetic theory, a plasma supports an infinite number of linear modes. With a few exceptions, these modes are heavily damped. The Alfvén wave and the magnetosonic solutions can still be identified in kinetic theory by their polarizations and dispersion relations (Stix 1992; Gary 1993; Klein 2013).

The solar wind is a turbulent and often collisionless magnetized plasma that carries a minor component of compressive fluctuations (Tu & Marsch 1995). In-situ observations indicate that density and field-strength fluctuations in the inertial range are anti-correlated (Bavassano & Bruno 1989; Yao et al. 2011; Howes et al. 2012; Klein et al. 2012; Yao et al. 2013a,b), suggesting that the compressions can be usefully modeled as slow modes under the assumption that strong plasma turbulence retains certain characteristics of linear plasma modes (Klein et al. 2012; Salem et al. 2012; Chen et al. 2013; Howes et al. 2014). Observations also show that the compressive fluctuations are more anisotropic than the Alfvénic fluctuations with $k_{\perp} \gg k_{\parallel}$ (Chen et al. 2012; Chen 2016), where k_{\perp} (k_{\parallel}) is the perpendicular (parallel) component of the wave vector with respect to the background magnetic field. Some literature interprets part of the compressive fluctuations as pressure-balanced structures (PBSs), i.e., structures in which the variation in the thermal pressure and the variation in the magnetic pressure balance so that the total pressure stays con-

stant (Burlaga & Ogilvie 1970; Vellante & Lazarus 1987; Burlaga et al. 1990; Zank et al. 1990; Zank & Matthaeus 1993; Marsch & Tu 1993; Tu & Marsch 1994; McComas et al. 1995; Ghosh et al. 1998; Reisenfeld et al. 1999; Bavassano et al. 2004; Yao et al. 2011; Verscharen et al. 2012; Narita & Marsch 2015; Yang et al. 2017). The large collisional mean free paths in the solar wind suggest that a kinetic description of these fluctuations is necessary that incorporates effects due to deviations from thermodynamic equilibrium, such as the commonly observed temperature anisotropies with respect to the background magnetic field (Marsch et al. 1982; Kasper 2002; Kasper et al. 2002; Hellinger et al. 2006; Bale et al. 2009; Chen et al. 2016; Verscharen et al. 2016).

In kinetic theory, the two modes most similar to the slow-magnetosonic mode are the ion-acoustic (IA) wave or a non-propagating (NP) mode depending on the plasma parameters (Howes et al. 2006). We refer to these modes as kinetic slow modes. The purpose of this work is to discuss the dispersion relations and the polarization properties of the IA wave, the NP mode, and the MHD slow mode. We use the fluctuations in the three lowest particle velocity moments (density, velocity, and pressure) as observable markers for the polarization of the compressive component of the solar-wind turbulence. By comparing our predictions for these markers with in-situ solar-wind observations, we distinguish between IA-mode-like, NP-mode-like, and MHD-slow-mode-like behavior. For more details on the IA and NP modes and a comprehensive derivation of their dispersion relations, we commend the extensive treatments by Howes et al. (2006), Schekochihin et al. (2009), and Kunz et al. (2015).

2. DISPERSION RELATIONS AND DAMPING RATES OF KINETIC SLOW MODES

Assuming large wavelengths ($k_{\perp}\rho_p \ll 1$), low frequencies ($\omega_r \ll \Omega_p$), and $k_{\perp} \gg k_{\parallel}$ in an electron-proton plasma, where

ω_p is the proton gyroradius, ω_r is the real part of the frequency ω , and Ω_p is the proton gyrofrequency, the gyrokinetic dispersion relation (see Appendix A for a sketch of the derivation) contains two distinct types of slow modes (Howes et al. 2006; Schekochihin et al. 2009). In the limit of low¹ $\beta_{\parallel p}$ and low $\beta_{\perp p}$, the slow-mode part of the dispersion relation describes IA waves. In the limit of high $\beta_{\parallel p}$ and high $\beta_{\perp p}$, the slow-mode part of the dispersion relation describes NP modes, where $\beta_{\parallel j} \equiv 8\pi n_0 j k_B T_{\parallel j} / B_0^2$, $\beta_{\perp j} \equiv \beta_{\parallel j} R_j$, n_0 is the background density of species j , and k_B is the Boltzmann constant. We define the temperature anisotropy of species j as $\Delta_j \equiv R_j - 1$, where $R_j \equiv T_{\perp j} / T_{\parallel j}$ and $T_{\perp j}$ ($T_{\parallel j}$) is the perpendicular (parallel) temperature of species j with respect to the background magnetic field \mathbf{B}_0 .

According to our derivation in Appendix A, IA waves fulfill the dispersion relation

$$\omega_r \simeq k_{\parallel} c_s, \quad (1)$$

where (Stix 1992; Gary 1993; Narita & Marsch 2015)

$$c_s \equiv \sqrt{\frac{3k_B T_{\parallel p} + k_B T_{\parallel e}}{m_p}} \quad (2)$$

is the ion-acoustic speed, and m_j is the particle mass of species j . As pointed out by Gary (1993), a comparison between Equation (2) with two-fluid theory, in which $\omega_r = k_{\parallel} C_F$ with the two-fluid sound speed

$$C_F \equiv \sqrt{\frac{\kappa_p k_B T_{\parallel p} + \kappa_e k_B T_{\parallel e}}{m_p}}, \quad (3)$$

implies that—to the degree to which an adiabatic behavior applies to the kinetic solution—the specific heat ratios in IA waves fulfill $\kappa_p = 3$ and $\kappa_e = 1$ for protons and electrons, respectively. From this point of view, protons behave like a one-dimensional adiabatic component due to their degree of freedom along \mathbf{B}_0 , while electrons behave like an isothermal component due to their large thermal speed compared to the wave phase speed. The imaginary part γ of the IA-wave frequency is given by

$$\gamma \simeq -|k_{\parallel}| c_s \sqrt{\pi} \frac{c_s^3}{w_{\parallel p}^3} \frac{e^{-c_s^2/w_{\parallel p}^2}}{1 + 3w_{\parallel p}^2/c_s^2}, \quad (4)$$

where $w_{\parallel p} \equiv \sqrt{2k_B T_{\parallel p} / m_p}$ is the parallel thermal speed of the protons. The derivation of Equations (1) and (4) requires the assumption that $T_{\parallel e} \gg T_{\parallel p}$ so that $\gamma \ll \omega_r$, although a comparison with numerical results in Figure 1 will show that Equation (1) is a good approximation even for $T_{\parallel e} \approx T_{\parallel p}$. Equation (4) reduces to the result given by Howes et al. (2006) for an isotropic plasma with $w_{\parallel p} \ll c_s$. The approximated IA dispersion relation in Equations (2) and (4) does not depend on $T_{\perp j}$ since the restoring force in the IA wave is solely due to the parallel pressure gradients of the protons and electrons (see also Basu 2008).

According to our derivation in Appendix A, NP modes fulfill the dispersion relation (see also Foote & Kulsrud 1979; Howes et al. 2006; Kunz et al. 2015) $\omega_r = 0$ and

$$\gamma \simeq -\frac{|k_{\parallel}| v_A}{R_p^2 \sqrt{\pi \beta_{\parallel p}}} (1 - \beta_{\perp p} \Delta_p - \beta_{\perp e} \Delta_e), \quad (5)$$

¹ We make the assumption that all inter-species temperature ratios as well as all R_j and $1/R_j$ are much less than $\sqrt{m_p/m_e}$.

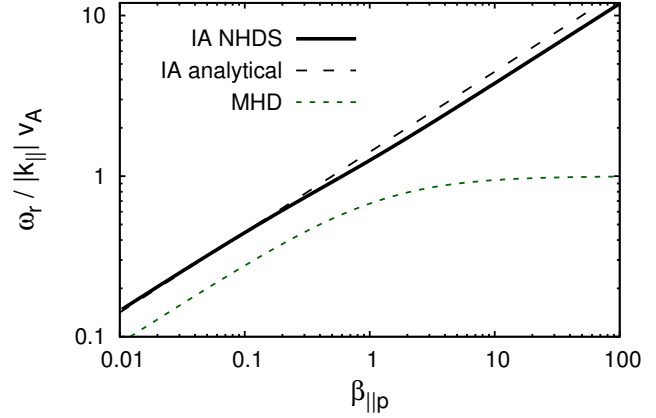


Figure 1. Comparison of the phase speeds of the IA mode from the fully-kinetic hot-plasma dispersion relation (NHDS) with Equation (1) in an electron-proton plasma. We use the parameters $T_{\parallel p} = T_{\parallel e}$, $\theta = 88^\circ$, $k_{\parallel} v_A / \Omega_p = 0.001$, and $R_p = R_e = 1$. The green dashed line shows Equation (7) with $\beta = \beta_{\parallel p}$ and $\kappa = 5/3$. The NP mode fulfills $\omega_r = 0$ exactly.

where $v_A \equiv B_0 / \sqrt{4\pi n_0 p m_p}$ is the proton Alfvén speed. The NP mode can become unstable ($\gamma > 0$) according to Equation (5) if

$$\beta_{\perp p} \Delta_p + \beta_{\perp e} \Delta_e > 1, \quad (6)$$

which is the mirror-mode instability criterion.

For the sake of brevity, we limit ourselves to the isotropic case for the following numerical evaluations of the dispersion relation. In Figure 1, we compare Equation (1) with numerical results of the fully-kinetic hot-plasma dispersion relation obtained with the numerical code NHDS (Verscharen et al. 2013). For reference, we show the MHD slow-mode dispersion relation,

$$\omega = k_{\parallel} v_A \frac{C}{\cos \theta}, \quad (7)$$

where

$$C \equiv \sqrt{\frac{1}{2} \left(1 + \frac{\kappa}{2} \beta \right) - \frac{1}{2} \left[\left(1 + \frac{\kappa}{2} \beta \right)^2 - 2\kappa \beta \cos^2 \theta \right]^{1/2}} \quad (8)$$

is the slow-magnetosonic speed, β is the ratio of thermal to magnetic pressure, and κ is the specific heat ratio. We set $\beta = \beta_{\parallel p}$ and $\kappa = 5/3$. We denote the angle between \mathbf{k} and \mathbf{B}_0 as θ . While the numerical and the analytical dispersion relations for the IA mode agree well with each other (even at high $\beta_{\parallel p}$), the MHD solution shows a significant deviation from the kinetic solutions, especially at high $\beta_{\parallel p}$.

In Figure 2, we compare Equations (4) and (5) with NHDS solutions. For this parameter set, the analytical results and the numerical results agree well for the NP mode at high $\beta_{\parallel p}$ as assumed in the derivation of Equation (4). Even at low $\beta_{\parallel p}$, Equation (4) and the numerical IA solution deviate from each other which is attributed to finite- $|\gamma/\omega_r|$ effects. Using this parameter set, the numerical damping rates of both modes are equal at $\beta_{\parallel p} \approx 0.3$.

3. POLARIZATION PROPERTIES AND RELATION TO PRESSURE-BALANCED STRUCTURES

We use the distinct polarization properties of the IA, NP, and MHD slow modes to identify the dominating mode in the solar wind. For that purpose, we define the dimensionless quantities ξ_j , χ_j , $\alpha_{\perp j}$, and $\alpha_{\parallel j}$ as the normalized observable amplitudes of fluctuations in the three lowest velocity

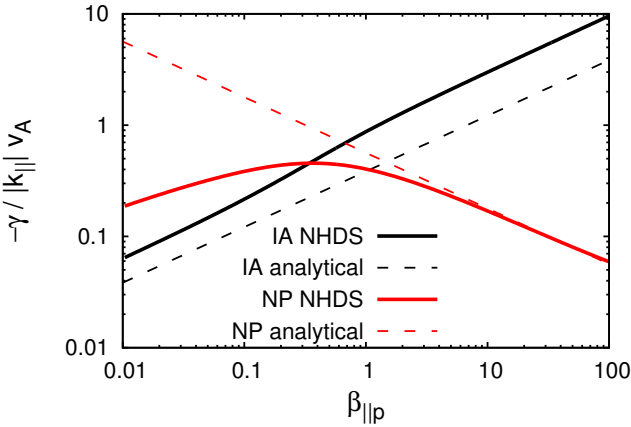


Figure 2. Damping rates of the IA wave and the NP mode in numerical solutions obtained with NHDS and according to Equations (4) and (5). The parameters are the same as in Figure 1.

moments:

$$\frac{\delta n_j}{n_{0j}} = \xi_j \frac{\delta B_{\parallel}}{B_0}, \quad (9)$$

where δn_j is the amplitude of fluctuations in the particle number density;

$$\frac{\delta U_{\parallel j}}{v_A} = \chi_j \frac{\delta B_{\parallel}}{B_0}, \quad (10)$$

where $\delta U_{\parallel j}$ is the amplitude of fluctuations in the \mathbf{B}_0 -parallel bulk velocity; and

$$\frac{\delta p_{\perp j}}{p_{B0}} = \alpha_{\perp j} \frac{\delta B_{\parallel}}{B_0}, \quad (11)$$

$$\frac{\delta p_{\parallel j}}{p_{B0}} = \alpha_{\parallel j} \frac{\delta B_{\parallel}}{B_0}, \quad (12)$$

where $\delta p_{\perp j}$ ($\delta p_{\parallel j}$) is the amplitude of fluctuations in the thermal pressure in the direction perpendicular (parallel) to \mathbf{B}_0 , and $p_{B0} \equiv B_0^2/8\pi$. We derive expressions for ξ_j , χ_j , $\alpha_{\perp j}$, and $\alpha_{\parallel j}$ in the gyrokinetic limit in Appendix B and give the MHD equivalents in Appendix C. Although all of these fluctuating moments are observable identifiers for the underlying plasma modes, the fluctuations in the total pressure play a decisive role due to the prominent observations of PBSs in the solar wind. Therefore, we define the normalized amplitude ψ_j of fluctuations in the thermal pressure as

$$\frac{\delta p_j}{p_{B0}} = \psi_j \frac{\delta B_{\parallel}}{B_0}. \quad (13)$$

where $p_{B0} \equiv B_0^2/8\pi$. With $p_j \equiv (2p_{\perp j} + p_{\parallel j})/3$, we find

$$\psi_j = \frac{2}{3} \alpha_{\perp j} + \frac{1}{3} \alpha_{\parallel j}. \quad (14)$$

In MHD, PBSs are associated with the MHD slow mode in the quasi-perpendicular limit (Tu & Marsch 1995; Kellogg & Horbury 2005; Klein 2013), suggesting that the IA wave and the NP mode be associated with the kinetic counterparts of PBSs. All wave solutions in the gyrokinetic approximation fulfill perpendicular pressure balance according to Equation (B1). However, the pressure balance commonly associated with PBSs implies that the sum of the total thermal pressures and the magnetic pressure remain constant:

$$p_p + p_e + p_B = \text{constant}, \quad (15)$$

where $p_B \equiv |\mathbf{B}|^2/8\pi$. Linearizing Equation (15) leads to

$$\frac{\delta p_p}{p_{B0}} + \frac{\delta p_e}{p_{B0}} + \frac{\delta p_B}{B_0} = 0. \quad (16)$$

With $\delta p_B \approx B_0 \delta B_{\parallel}/4\pi$, pressure balance according to Equation (15) is then achieved if

$$\psi \equiv \psi_p + \psi_e = -2. \quad (17)$$

The quantities ξ_j , χ_j , $\alpha_{\perp j}$, $\alpha_{\parallel j}$, ψ_j , and ψ are complex quantities. For their comparison with observations in Section 3.2, we express them in terms of their magnitude, $|\cdot|$, and phase angle, $\arg(\cdot)$.

3.1. Observational Methods

For the observational analysis, we use data from the Wind spacecraft (Acuña et al. 1995) in the solar wind at 1 AU. We use magnetic-field data from the MFI instrument (Lepping et al. 1995) at 3-second resolution. For the particles, we use the ground-calculated moments from the 3DP instrument (Lin et al. 1995), at 24-second resolution for the ions and at 98-second resolution for the electrons. We split the data from the period 1 July 2004 to 31 December 2014 into non-overlapping 1-hour intervals and linearly interpolate data gaps. We exclude intervals with data gaps greater than 5% from the analysis.

In each 1-hour interval, we determine the mean and fluctuating values in order to calculate the polarization properties ξ_p , χ_p , and ψ , defined in Section 3. We determine n_{0p} and \mathbf{B}_0 as averages over each interval and determine v_A and p_{B0} from those averages. We also determine $\beta_{\parallel p}$ from the average density, magnetic field, and parallel temperature of the interval. For the amplitudes of ξ_p , χ_p , and ψ , we calculate the rms values of each quantity. For the phases of ξ_p , χ_p , and ψ , we calculate the wavelet coherence spectrum,

$$C_{\delta A, \delta |\mathbf{B}|/B_0}(a, b) \equiv S [W_{\delta A}^*(a, b) W_{\delta |\mathbf{B}|/B_0}(a, b)], \quad (18)$$

(Torrence & Compo 1998) for each quantity $\delta A \in (\delta n_p/n_{0p}, \delta U_{\parallel p}/v_A, \delta p_{\perp j}/p_{B0}, \delta p_{\parallel j}/p_{B0})$, where $W_X(a, b)$ is the continuous Morlet-wavelet transform of X at scales a and positions b , and S is a smoothing parameter in time and scale. The phase is defined as the coherence phase,

$$\text{phase} = \tan^{-1} \frac{\text{Im} [C_{\delta A, \delta |\mathbf{B}|/B_0}(a, b)]}{\text{Re} [C_{\delta A, \delta |\mathbf{B}|/B_0}(a, b)]}. \quad (19)$$

We then take the average over scales between 1 hour and 15 minutes. At shorter timescales, instrument noise would contaminate our results. In our data analysis, we use $\delta |\mathbf{B}|$ instead of δB_{\parallel} in the definitions of ξ_p , χ_p , and ψ in order to reduce uncertainties in the determination of the \mathbf{B}_0 -parallel direction. In the limit in which our linear analysis is valid, $\delta |\mathbf{B}| \simeq \delta B_{\parallel}$. We then create two-dimensional histograms in the ξ_p - $\beta_{\parallel p}$, χ_p - $\beta_{\parallel p}$, and ψ - $\beta_{\parallel p}$ planes, binning the data logarithmically in $\beta_{\parallel p}$ and ξ_p , and linearly in χ_p and ψ . Lastly, we normalize each column of data in the histogram at a constant $\beta_{\parallel p}$ by the peak counts in that column, so each column is independently normalized to show the peak in the variable at a fixed $\beta_{\parallel p}$.

3.2. Results

According to observations (e.g., Kasper 2002; Kasper et al. 2002; Hellinger et al. 2006; Bale et al. 2009; Chen et al. 2016), the mirror-mode and firehose thresholds set approximate upper and lower limits on R_p . Therefore, we set the maximum

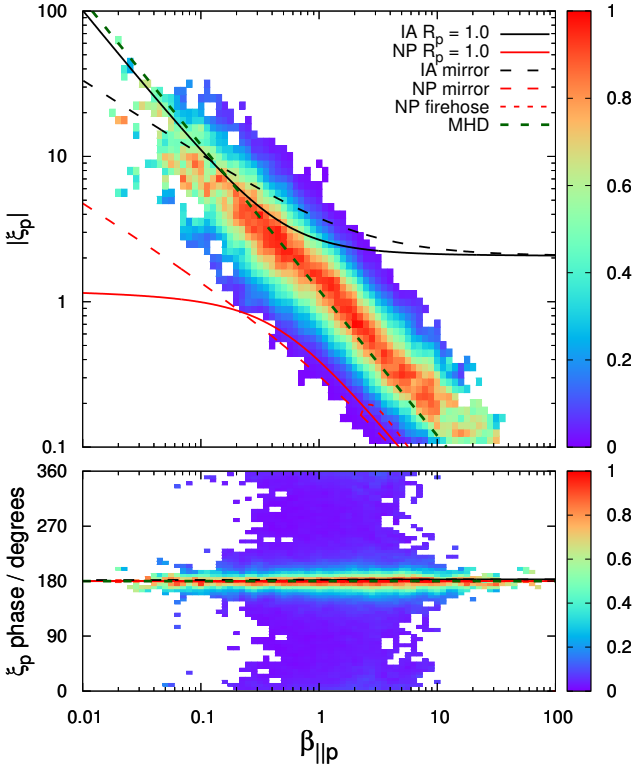


Figure 3. ξ_p as a function of $\beta_{\parallel p}$. The lines show our theoretical results and the color-coded dots show the linearly scaled column-normalized data distribution in the ξ_p - $\beta_{\parallel p}$ plane. The top panel shows $|\xi_p|$, and the bottom panel shows the phase angle between δn_p and δB_{\parallel} .

and minimum values of R_p in our calculations to the values that fulfill Equation (6) (labeled as “IA/NP mirror”) or Equation (A23) (labeled as “NP firehose”), after replacing the inequality signs with equality signs. These curves identify the extreme values for ξ_p , χ_p , and ψ in an anisotropic plasma. For comparison, we also include the results from isotropic MHD as derived in Appendix C.

We show the numerical and observational results for the zeroth velocity moment (ξ_p) as functions of $\beta_{\parallel p}$ in Figure 3. Our theoretical results indicate that the vast majority of the data exhibit phase-angles of $\sim 180^\circ$, showing a strong anti-correlation between δn_p and δB_{\parallel} . The MHD prediction is shown for $\kappa = 5/3$. Although the NP-mode prediction agrees better with the observations at large $\beta_{\parallel p}$ than the IA-mode prediction and vice versa, the MHD solution shows the best agreement overall with the observations of ξ_p in both absolute value and phase. In the highly-oblique limit, Equation (C5) leads to $\xi_{\text{MHD}} \rightarrow -2/(\kappa \beta_{\parallel p})$. A best fit to the data in Figure 3 using this limit shows that the observed ξ_p -behavior of the large-scale compressive fluctuations in the solar wind corresponds to the MHD behavior of highly-oblique slow modes with

$$\kappa = 1.4412 \pm 0.0036, \quad (20)$$

where the error margin represents the statistical error of the fit only.

We compare our predictions for the first velocity moment (χ_p) with observations in Figure 4. Our theoretical results show that $|\chi_p|$ is much greater in the IA mode than in the NP mode. While the theoretical NP-mode solutions for $R_p = 1$ and at the firehose threshold exhibit a 90° -phase shift between $\delta U_{\parallel p}$ and δB_{\parallel} , the observations predominantly exhibit a phase

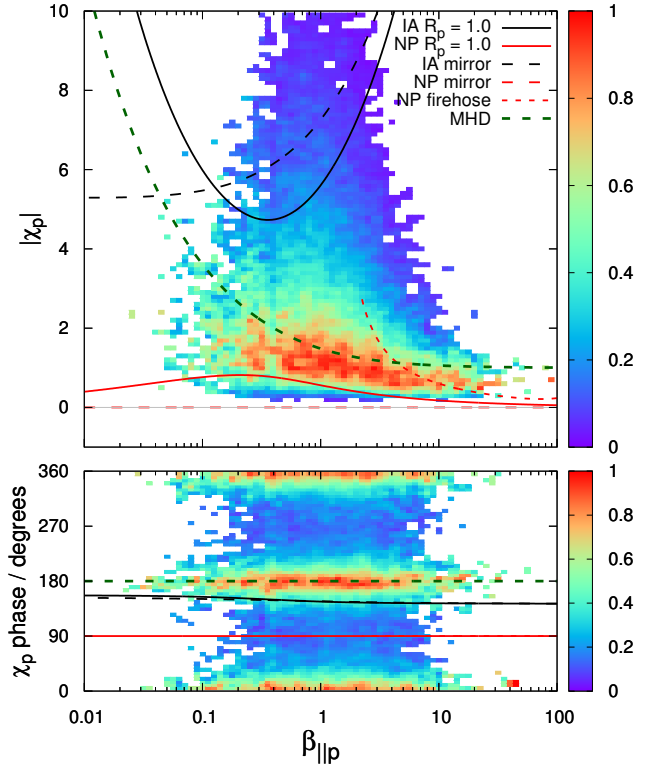


Figure 4. χ_p as a function of $\beta_{\parallel p}$. The lines show our theoretical results and the color-coded dots show the linearly scaled column-normalized data distribution in the χ_p - $\beta_{\parallel p}$ plane. The top panel shows $|\chi_p|$, and the bottom panel shows the phase angle between $\delta U_{\parallel p}$ and δB_{\parallel} .

shift of $\sim 180^\circ$ and $\sim 0^\circ$. Like in the case of ξ_p , the MHD solution shows the best agreement with the observations of χ_p in both absolute value and phase. We note, however, that the measurement of χ_p is prone to *Alfvénic leakage*, which increases the uncertainty of this observation. Alfvénic leakage is a result of the dominant Alfvénic fluctuations and their characteristic (anti-)correlation between $\delta \mathbf{B}$ and $\delta \mathbf{U}_p$. Fluctuations on time scales comparable to the time scale we use in defining \mathbf{B}_0 introduce inaccuracies to our projections of $\delta \mathbf{B}$ and $\delta \mathbf{U}_p$ onto the \mathbf{B}_0 -parallel direction. Consequently, some of the strong transversal Alfvénic fluctuations in $\delta \mathbf{B}$ and $\delta \mathbf{U}_p$ appear as partly field-parallel. Alfvénic leakage creates signals at phases of both $\sim 180^\circ$ and $\sim 0^\circ$.

Lastly, we show our results for ψ in Figure 5. The IA wave and the NP mode do not fulfill Equation (17). The MHD prediction exhibits full pressure balance and a reasonable agreement with the observations, especially at $\beta_{\parallel p} \gtrsim 0.5$.

4. DISCUSSION AND CONCLUSIONS

The long-wavelength kinetic slow mode is associated with two types of compressive modes: the ion-acoustic (IA) wave and a non-propagating (NP) mode, both of which exhibit an anti-correlation between δn_j and $\delta |\mathbf{B}|$. A comparison of the damping rates of the IA mode and the NP mode suggests that the IA mode is the dominating kinetic slow mode at low $\beta_{\parallel p}$, while the NP mode is the dominating kinetic slow mode at high $\beta_{\parallel p}$. Temperature anisotropies alter the dispersion relations and the damping behavior of slow modes in kinetic plasmas and can drive the NP mode (i.e., the mirror mode) unstable.

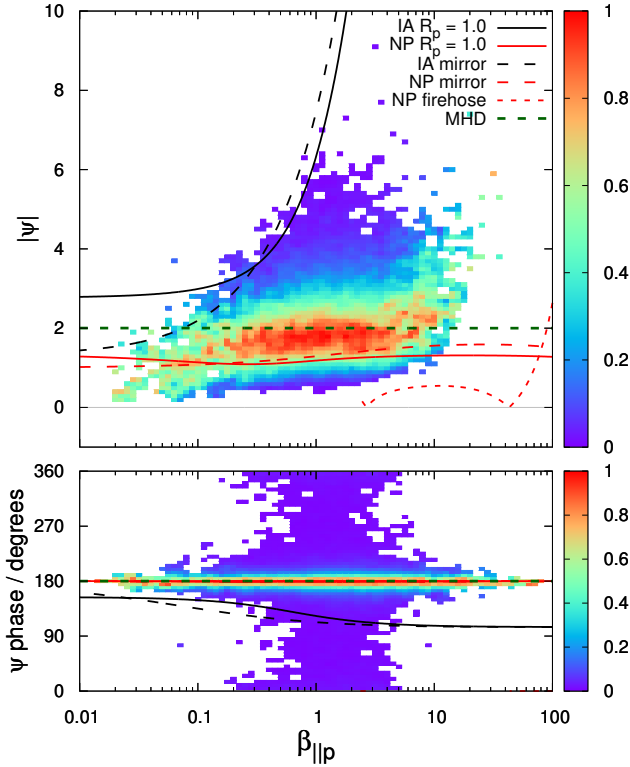


Figure 5. ψ as a function of $\beta_{\parallel p}$. The lines show our theoretical results and the color-coded dots show the linearly scaled column-normalized data distribution in the ψ - $\beta_{\parallel p}$ plane. The top panel shows $|\psi|$, and the bottom panel shows the phase angle between $(\delta p_p + \delta p_e)$ and δB_{\parallel} .

While MHD does not account for the NP mode² or kinetic damping of slow modes, the $\beta_{\parallel p}$ -dependence of ω_r for the IA wave is roughly represented by MHD at low $\beta_{\parallel p}$. At high $\beta_{\parallel p}$, however, the MHD approximation does not agree with the dispersion relations of either type of kinetic slow modes. Our careful comparison of theoretical predictions for the three lowest particle velocity moments associated with IA, NP, and MHD slow modes with observations suggests that the compressive component of the solar-wind fluctuations is not IA-wave or NP-mode like. Our MHD slow-mode calculation predicts the observed $\beta_{\parallel p}$ -dependence of ψ well, corroborating the notion that the MHD slow mode is a potential candidate for PBSs observed in the solar wind (Kellogg & Horbury 2005; Yao et al. 2013a,b).

Klein et al. (2012) compare the normalized correlation between δn_p and δB_{\parallel} in a synthetic spacecraft dataset based on a combination of slow and fast modes with observations. In their analysis, the synthetic data based on a superposition of critically-balanced IA waves explain the observed $\beta_{\parallel p}$ -dependence of the normalized correlation for $0.1 \leq \beta_{\parallel p} \leq 10$ better than the synthetic data based on a superposition of MHD waves. Applying Klein et al.'s (2012) synthetic-spacecraft method to our markers ξ_p , χ_p , and ψ over a wider $\beta_{\parallel p}$ -range using a composition of IA, NP, and other kinetic and MHD modes may lead to observable predictions that clarify the nature of the compressive component of the solar-wind turbulence. In addition, appropriate fully nonlinear turbulence simulations can determine the behavior of slow modes in a

² We note that the MHD entropy mode shares certain characteristics with the NP kinetic slow mode; however, there are significant differences between these modes. For example, the MHD entropy mode has no fluctuations in \mathbf{B} .

turbulent background. However, these studies are beyond the scope of our work.

Although the large collisional mean free paths in the solar wind suggest a preference of kinetic models over MHD models, our observations agree better with the MHD solutions than with the IA-wave or NP-mode solutions. Our study, therefore, suggests that the large-scale compressive fluctuations in the solar wind behave more fluid-like than kinetic-slow-mode-like. Even the restriction of our data to measurements with low collisional age, $A_c < 0.1$ (Kasper et al. 2008; Bourouaine et al. 2011), or a reduction of the average time from 1-hour intervals to 10-minute intervals does not change this result (plots for these restrictions are not shown). This discovery suggests that some fundamental process, which remains to be identified, creates an effective collisionality and thus the requirements for the application of the MHD framework. Possible candidates for such processes include the inhibition of the development of fine structures and damping due to anti-phase-mixing (see Section 5.3 in Schekochihin et al. 2016), scattering by wave-particle collisions and kinetic instabilities (Riquelme et al. 2015; Kunz et al. 2016; Riquelme et al. 2016; Verscharen et al. 2016; Yoon 2016), or the isotropization due to the dissipation of electric fluctuations (Bale et al. 2005). These processes may be scale-dependent, so that a faster measurement cadence could reveal a more kinetic-slow-mode-like behavior on short time scales. The instrumentation on the upcoming missions Solar Orbiter and Solar Probe Plus will provide appropriate measurements for such a scale-dependent study.

We thank Ben Chandran and Kris Klein for very helpful discussions. DV is supported by NSF/SHINE grant AGS-1460190 and NASA grant NNX16AG81G. CHKC is supported by an STFC Ernest Rutherford Fellowship.

APPENDIX

A. DERIVATION OF THE DISPERSION RELATION IN THE GYROKINETIC APPROXIMATION

In this appendix, we sketch the derivation of the gyrokinetic slow-mode dispersion relation in an anisotropic plasma combining the derivations given by Howes et al. (2006) and Kunz et al. (2015) and using their notation. For simplicity, we assume a bi-Maxwellian background distribution function:

$$f_{0j} = \frac{n_{0j}}{\pi^{3/2} w_{\perp j}^2 w_{\parallel j}^2} \exp\left(-\frac{v_{\perp}^2}{w_{\perp j}^2} - \frac{v_{\parallel}^2}{w_{\parallel j}^2}\right), \quad (A1)$$

where $w_{\perp j} \equiv \sqrt{2k_B T_{\perp j}/m_j}$. In the gyrokinetic ordering ($\epsilon \sim k_{\parallel}/k_{\perp} \sim \omega/\Omega_j \sim \dots \ll 1$), the distribution function is decomposed as

$$f_j = f_{0j} + \delta f_{1j} + h_j + \dots, \quad (A2)$$

where

$$\delta f_{1j} \equiv -\frac{q_j}{k_B T_{\perp j}} \left(\phi + \frac{v_{\parallel} A_{\parallel}}{c} \Delta_j \right) f_{0j} \quad (A3)$$

is the Boltzmann response, h_j is the gyrokinetic response, q_j is the charge of species j , ϕ is the electrostatic potential, \mathbf{A} is the vector potential, and c is the speed of light. The collisionless gyrokinetic equation to first order in ϵ is then given

by

$$\begin{aligned} \frac{\partial h_j}{\partial t} + v_{\parallel} \frac{\partial h_j}{\partial z} + \frac{c}{B_0} \{ \langle \chi \rangle_{\mathbf{R}}, h_j \} \\ = \frac{q_j f_{0j}}{k_B T_{\perp j}} \frac{\partial \langle \chi \rangle_{\mathbf{R}}}{\partial t} - \frac{q_j f_{0j} \Delta_j}{k_B T_{\perp j}} v_{\parallel} \frac{\partial \langle \chi \rangle_{\mathbf{R}}}{\partial z}, \end{aligned} \quad (\text{A4})$$

where $\langle \chi \rangle_{\mathbf{R}} \equiv \langle \phi - \mathbf{v} \cdot \mathbf{A}/c \rangle_{\mathbf{R}}$ and $\{ \cdot, \cdot \}$ is the Poisson bracket. The symbol $\langle \cdot \rangle_{\mathbf{R}}$ indicates the ring average at the fixed gyro-center \mathbf{R} of species j .

Applying a plane-wave ansatz to h_j allows us to express the ring average in terms of Bessel functions of order m , $J_{mj} \equiv$

$J_m(k_{\perp} v_{\perp} / \Omega_j)$, which yields

$$\begin{aligned} h_j = \frac{q_j f_{0j}}{k_B T_{\perp j}} \left\{ \left(\omega + k_{\parallel} v_{\parallel} \Delta_j \right) J_{0j} \frac{A_{\parallel}}{k_{\parallel} c} + \left(\frac{\omega R_j}{\omega - k_{\parallel} v_{\parallel}} - \Delta_j \right) \right. \\ \left. \times \left[J_{0j} \left(\phi - \frac{\omega A_{\parallel}}{k_{\parallel} c} \right) + \frac{k_B T_{\perp j}}{q_j} \frac{2v_{\perp}^2}{w_{\perp j}^2} J_{1j} \Omega_j \frac{\delta B_{\parallel}}{B_0} \right] \right\}. \end{aligned} \quad (\text{A5})$$

The three lowest velocity moments of the fluctuating gyrokinetic distribution function to first order (i.e., the Boltzmann response and the gyrokinetic response) describe the fluctuations in density, bulk velocity, and the perpendicular and parallel thermal pressures as:

$$\delta n_j = \frac{q_j n_{0j}}{k_B T_{\perp j}} \left\{ \Gamma_{0j} \frac{\omega A_{\parallel}}{k_{\parallel} c} - \phi - (R_j \zeta_j Z_j + \Delta_j) \left[\Gamma_{0j} \left(\phi - \frac{\omega A_{\parallel}}{k_{\parallel} c} \right) + \Gamma_{1j} \frac{k_B T_{\perp j}}{q_j} \frac{\delta B_{\parallel}}{B_0} \right] \right\}, \quad (\text{A6})$$

$$\delta U_{\parallel j} = \frac{q_j}{k_B T_{\perp j}} \left\{ \frac{w_{\parallel j}^2 A_{\parallel}}{2c} \Delta_j (\Gamma_{0j} - 1) - \frac{\omega}{k_{\parallel}} R_j (\zeta_j Z_j + 1) \left[\Gamma_{0j} \left(\phi - \frac{\omega A_{\parallel}}{k_{\parallel} c} \right) + \Gamma_{1j} \frac{k_B T_{\perp j}}{q_j} \frac{\delta B_{\parallel}}{B_0} \right] \right\}, \quad (\text{A7})$$

$$\delta p_{\perp j} = q_j n_{0j} \left\{ \Gamma_{3j} \frac{\omega A_{\parallel}}{k_{\parallel} c} - \phi - (R_j \zeta_j Z_j + \Delta_j) \left[\Gamma_{3j} \left(\phi - \frac{\omega A_{\parallel}}{k_{\parallel} c} \right) + \Gamma_{4j} \frac{k_B T_{\perp j}}{q_j} \frac{\delta B_{\parallel}}{B_0} \right] \right\}, \quad (\text{A8})$$

$$\delta p_{\parallel j} = q_j n_{0j} \frac{1}{R_j} \left\{ \Gamma_{0j} \frac{\omega A_{\parallel}}{k_{\parallel} c} - \phi - [2R_j \zeta_j^2 (1 + \zeta_j Z_j) + \Delta_j] \left[\Gamma_{0j} \left(\phi - \frac{\omega A_{\parallel}}{k_{\parallel} c} \right) + \Gamma_{1j} \frac{k_B T_{\perp j}}{q_j} \frac{\delta B_{\parallel}}{B_0} \right] \right\}, \quad (\text{A9})$$

where we evaluate the integrals over v_{\perp} in terms of the modified Bessel functions I_m with $\Gamma_{0j} \equiv I_0(\lambda_j) e^{-\lambda_j}$, $\Gamma_{1j} \equiv [I_0(\lambda_j) - I_1(\lambda_j)] e^{-\lambda_j}$, $\Gamma_{2j} \equiv 2 [I_0(\lambda_j) - I_1(\lambda_j)] e^{-\lambda_j}$, $\Gamma_{3j} \equiv \Gamma_{0j} + \lambda_j \Gamma'_{0j}$, and $\Gamma_{4j} \equiv 2\Gamma_{1j} + \lambda_j \Gamma'_{1j}$ with the argument $\lambda_j \equiv k_{\perp} w_{\perp j}^2 / 2\Omega_j^2$. We express the integrals over v_{\parallel} in terms of the standard plasma dispersion function (Fried & Conte 1961)

$$Z_j \equiv \frac{1}{\sqrt{\pi}} \int_{\mathcal{C}} \frac{e^{-t^2}}{t - \zeta_j} dt \quad (\text{A10})$$

along the Landau contour \mathcal{C} , where $\zeta_j \equiv \omega / |k_{\parallel}| w_{\parallel j}$.

With these relations, the condition of quasi-neutrality, the parallel component of Ampère's law, and the perpendicular components of Ampère's law ($\nabla_{\perp} \delta B_{\parallel} = (4\pi/c) \hat{\mathbf{z}} \times \delta \mathbf{j}$), where $\delta \mathbf{j}$ is the fluctuating part of the current density, yield:

$$\sum_j q_j \delta n_j = 0. \quad (\text{A11})$$

$$k_{\perp}^2 A_{\parallel} - \frac{4\pi}{c} \sum_j q_j n_{0j} \delta U_{\parallel j} = 0, \quad (\text{A12})$$

and

$$\begin{aligned} \frac{\delta B_{\parallel}}{B_0} + \frac{4\pi}{B_0^2} \sum_j q_j n_{0j} \left\{ \Gamma_{1j} \frac{\omega A_{\parallel}}{k_{\parallel} c} - (R_j \zeta_j Z_j + \Delta_j) \right. \\ \left. \times \left[\Gamma_{1j} \left(\phi - \frac{\omega A_{\parallel}}{k_{\parallel} c} \right) + \Gamma_{2j} \frac{k_B T_{\perp j}}{q_j} \frac{\delta B_{\parallel}}{B_0} \right] \right\} = 0, \end{aligned} \quad (\text{A13})$$

As shown by Howes et al. (2006), we can write Equa-

tions (A11) through (A13) as

$$\begin{pmatrix} A & A-B & C \\ A-B & A-B-\frac{P}{\bar{\omega}^2} & C+E \\ C & C+E & D-\frac{2}{\beta_{\perp p}} \end{pmatrix} \begin{pmatrix} \phi \\ -\frac{\omega A_{\parallel}}{k_{\parallel} c} \\ \frac{k_B T_{\perp p}}{q_p} \frac{\delta B_{\parallel}}{B_0} \end{pmatrix} = 0 \quad (\text{A14})$$

for $n_{0p} = n_{0e}$, where

$$\begin{aligned} A &\equiv 1 + (R_p \zeta_p Z_p + \Delta_p) \Gamma_{0p} \\ &+ \frac{T_{\perp p}}{T_{\perp e}} [1 + (R_e \zeta_e Z_e + \Delta_e) \Gamma_{0e}], \end{aligned} \quad (\text{A15})$$

$$B \equiv 1 - \Gamma_{0p} + \frac{T_{\perp p}}{T_{\perp e}} (1 - \Gamma_{0e}), \quad (\text{A16})$$

$$C \equiv (R_p \zeta_p Z_p + \Delta_p) \Gamma_{1p} - (R_e \zeta_e Z_e + \Delta_e) \Gamma_{1e}, \quad (\text{A17})$$

$$D \equiv (R_p \zeta_p Z_p + \Delta_p) \Gamma_{2p} + \frac{T_{\perp e}}{T_{\perp p}} (R_e \zeta_e Z_e + \Delta_e) \Gamma_{2e}, \quad (\text{A18})$$

$$E \equiv \Gamma_{1p} - \Gamma_{1e}, \quad (\text{A19})$$

$$\begin{aligned} P &\equiv \lambda_p + \frac{1}{2} \beta_{\parallel p} \Delta_p (1 - \Gamma_{0p}) \\ &+ \frac{T_{\perp p}}{T_{\perp e}} \frac{1}{2} \beta_{\parallel e} \frac{m_p}{m_e} \Delta_e (1 - \Gamma_{0e}), \end{aligned} \quad (\text{A20})$$

and $\bar{\omega} \equiv \omega / |k_{\parallel}| v_A$. Setting the determinant of the matrix in Equation (A14) to zero leads to the nontrivial solutions of the gyrokinetic dispersion relation, which fulfill

$$\left(\frac{PA}{\bar{\omega}^2} - AB + B^2 \right) \left(\frac{2A}{\beta_{\perp p}} - AD + C^2 \right) = (AE + BC)^2. \quad (\text{A21})$$

The term on the right-hand side of Equation (A21) represents coupling terms that can be neglected for long wavelengths. In

the long-wavelength limit ($\lambda_j \ll 1$), we apply the approximations $\Gamma_{0j} \simeq 1 - \lambda_j$, $\Gamma_{1j} \simeq 1 - 3\lambda_j/2$, and $\Gamma_{2j} \simeq 2 - 3\lambda_j$. Furthermore, we neglect all terms $\sim m_e/m_p$ given the assumed constraints on the temperature ratios.

The first term on the left-hand side represents the Alfvén solution, and the second term represents the slow-mode solution. In the long-wavelength limit, the Alfvén branch reduces to $P = \bar{\omega}^2 \lambda_p$, which leads to the Alfvén dispersion relation

$$\omega = \pm k_{\parallel} v_A \left(1 + \frac{\beta_{\parallel p}}{2} \Delta_p + \frac{\beta_{\parallel e}}{2} \Delta_e \right)^{1/2}. \quad (\text{A22})$$

If the expression in parentheses in Equation (A22) becomes negative, this root of the dispersion relation describes the firehose instability with the instability criterion

$$\beta_{\parallel p} - \beta_{\perp p} + \beta_{\parallel e} - \beta_{\perp e} > 2. \quad (\text{A23})$$

The slow-mode branch can be analytically simplified in two limits. In the low- $\beta_{\perp p}$ limit, the slow-mode dispersion relation becomes $A = 0$. Using the expansion

$$Z_p \simeq i\sqrt{\pi} e^{-\zeta_p^2} - \frac{1}{\zeta_p} - \frac{1}{2\zeta_p^3} - \frac{3}{4\zeta_p^5} \quad (\text{A24})$$

and $\zeta_e Z_e \ll 1$ leads to

$$\frac{T_{\parallel p}}{T_{\parallel e}} + i\sqrt{\pi} \frac{\omega}{|k_{\parallel}| w_{\parallel p}} e^{-\omega^2/k_{\parallel}^2 w_{\parallel p}^2} - \frac{k_{\parallel}^2 w_{\parallel p}^2}{2\omega^2} - \frac{3k_{\parallel}^4 w_{\parallel p}^4}{4\omega^4} = 0. \quad (\text{A25})$$

Under the assumption that $T_{\parallel e} \gg T_{\parallel p}$ and $\gamma \ll \omega_r$, the real part of Equation (A25) leads to Equation (1), and the imaginary part of Equation (A25) leads to Equation (4).

In the high- $\beta_{\perp p}$ limit, the slow-mode dispersion relation becomes $2/\beta_{\perp p} = D$. Using the expansion $Z_p \simeq i\sqrt{\pi}$ and $\zeta_e \ll \zeta_p$, this solution leads to the dispersion relation of the NP mode, $\omega_r = 0$ and Equation (5).

B. DERIVATION OF MOMENT FLUCTUATIONS IN THE GYROKINETIC APPROXIMATION

The perpendicular component of Ampère's law in gyrokinetics implies pressure balance in the form

$$\nabla_{\perp} \left(\frac{B_0 \delta B_{\parallel}}{4\pi} + \delta \mathbf{P}_{\perp} \right) = 0, \quad (\text{B1})$$

where

$$\delta \mathbf{P}_{\perp} \equiv \sum_j m_j \int \langle \mathbf{v}_{\perp} \mathbf{v}_{\perp} h_j \rangle_{\mathbf{r}} d^3 v \quad (\text{B2})$$

is the perpendicular pressure tensor and $\langle \cdot \rangle_{\mathbf{r}}$ is the ring average at fixed position \mathbf{r} . Fluctuations in the total thermal pressure are due to fluctuations in the density as well as the perpendicular and parallel temperatures of all species.

For a given solution to the dispersion relation, Equation (A14) provides the polarization relations that connect the three amplitudes ϕ , A_{\parallel} , and δB_{\parallel} :

$$\begin{pmatrix} \phi \\ \omega A_{\parallel} \\ k_{\parallel} c \end{pmatrix} = \begin{pmatrix} L_{\phi} \\ L_A \\ 1 \end{pmatrix} \frac{k_B T_{\perp p}}{q_p} \frac{\delta B_{\parallel}}{B_0}, \quad (\text{B3})$$

where

$$L_{\phi} = \frac{\left(D - \frac{2}{\beta_{\perp p}} \right) (A - B - \frac{P}{\bar{\omega}^2}) - (C + E)^2}{\frac{PC}{\bar{\omega}^2} + AE - BE} \quad (\text{B4})$$

and

$$L_A = \frac{\left(D - \frac{2}{\beta_{\perp p}} \right) (A - B) - C(C + E)}{\frac{PC}{\bar{\omega}^2} + AE - BE}. \quad (\text{B5})$$

With Equations (A6) through (A9), (B4), and (B5), we find for the normalized fluctuations in the three lowest velocity moments:

$$\begin{aligned} \xi_j &= \tau_j \left\{ \Gamma_{0j} L_A - L_{\phi} - (R_j \zeta_j Z_j + \Delta_j) \right. \\ &\quad \left. \times \left[\Gamma_{0j} (L_{\phi} - L_A) + \frac{\Gamma_{1j}}{\tau_j} \right] \right\}, \end{aligned} \quad (\text{B6})$$

$$\begin{aligned} \chi_j &= \tau_j \left\{ \frac{1}{2} \frac{k_{\parallel} v_A}{\omega} \frac{m_p}{m_j} \beta_{\parallel j} \Delta_j (\Gamma_{0j} - 1) L_A \right. \\ &\quad \left. - \frac{\omega}{k_{\parallel} v_A} R_j (1 + \zeta_j Z_j) \left[\Gamma_{0j} (L_{\phi} - L_A) + \frac{\Gamma_{1j}}{\tau_j} \right] \right\}, \end{aligned} \quad (\text{B7})$$

$$\begin{aligned} \alpha_{\perp j} &= \tau_j \beta_{\perp j} \left\{ \Gamma_{3j} L_A - L_{\phi} - (R_j \zeta_j Z_j + \Delta_j) \right. \\ &\quad \left. \times \left[\Gamma_{3j} (L_{\phi} - L_A) + \frac{\Gamma_{4j}}{\tau_j} \right] \right\}, \end{aligned} \quad (\text{B8})$$

$$\begin{aligned} \alpha_{\parallel j} &= \tau_j \beta_{\parallel j} \left\{ \Gamma_{0j} L_A - L_{\phi} \right. \\ &\quad \left. - [2R_j \zeta_j^2 (1 + \zeta_j Z_j) + \Delta_j] \right. \\ &\quad \left. \times \left[\Gamma_{0j} (L_{\phi} - L_A) + \frac{\Gamma_{1j}}{\tau_j} \right] \right\}, \end{aligned} \quad (\text{B9})$$

where

$$\tau_j \equiv \frac{q_j T_{\perp p}}{q_p T_{\perp j}}. \quad (\text{B10})$$

We then calculate the factor ψ with Equation (14) after solving Equation (A14) numerically (i.e., without approximating Γ_{ij} and Z_j) for ω , L_{ϕ} , and L_A . In the marginally-stable case for the mirror-mode instability, the NP mode fulfills $\omega = 0$, $L_{\phi} = -C/A$, $L_A = 0$, and Equation (6).

C. MHD POLARIZATION RELATIONS

Linearizing the ideal adiabatic MHD equations for a proton fluid,

$$\frac{\partial n_p}{\partial t} + \nabla \cdot (n_p \mathbf{U}) = 0, \quad (\text{C1})$$

$$\frac{\partial \mathbf{U}}{\partial t} + (\mathbf{U} \cdot \nabla) \mathbf{U} = -\frac{\nabla p}{n_p m_p} + \frac{1}{4\pi n_p m_p} [(\nabla \times \mathbf{B}) \times \mathbf{B}], \quad (\text{C2})$$

$$\frac{\partial \mathbf{B}}{\partial t} = \nabla \times (\mathbf{U} \times \mathbf{B}), \quad (\text{C3})$$

$$p n_p^{-\kappa} = \text{constant}, \quad (\text{C4})$$

where \mathbf{U} is the fluid velocity and p is the pressure, leads to slow magnetosonic wave solutions with the dispersion relation given by Equations (7) and (8). Combining Equations (C1) through (C4) with Equations (9), (10), and (13) leads to

$$\xi_{\text{MHD}} = \frac{C_-^2}{C_-^2 - \frac{\kappa}{2} \beta_{\parallel p} \cos^2 \theta}, \quad (\text{C5})$$

$$\chi_{\text{MHD}} = \frac{C_- \cos \theta}{C_-^2 - \frac{\kappa}{2} \beta_{\parallel p} \cos^2 \theta} \frac{\kappa}{2} \beta_{\parallel p} \quad (\text{C6})$$

(Verscharen et al. 2016), and

$$\psi_{\text{MHD}} = \kappa \beta_{\parallel p} \xi_{\text{MHD}}. \quad (\text{C7})$$

We note that ψ_{MHD} describes the effect of the total isotropic pressure instead of the proton partial pressure alone.

REFERENCES

Acuña, M. H., Ogilvie, K. W., Baker, D. N., et al. 1995, *Space Sci. Rev.*, 71, 5

Bale, S. D., Kasper, J. C., Howes, G. G., et al. 2009, *Phys. Rev. Lett.*, 103, 211101

Bale, S. D., Kellogg, P. J., Mozer, F. S., Horbury, T. S., & Reme, H. 2005, *Phys. Rev. Lett.*, 94, 215002

Basu, B. 2008, *Phys. Plasmas*, 15, 042108

Bavassano, B., & Bruno, R. 1989, *J. Geophys. Res.*, 94, 11977

Bavassano, B., Pietropaolo, E., & Bruno, R. 2004, *Ann. Geophys.*, 22, 689

Bourouaine, S., Marsch, E., & Neubauer, F. M. 2011, *ApJ*, 728, L3

Burlaga, L. F., & Ogilvie, K. W. 1970, *Solar Phys.*, 15, 61

Burlaga, L. F., Scudder, J. D., Klein, L. W., & Isenberg, P. A. 1990, *J. Geophys. Res.*, 95, 2229

Chen, C. H. K. 2016, *J. Plasma Phys.*, 82, 535820602

Chen, C. H. K., Boldyrev, S., Xia, Q., & Perez, J. C. 2013, *Phys. Rev. Lett.*, 110, 225002

Chen, C. H. K., Mallet, A., Schekochihin, A. A., et al. 2012, *ApJ*, 758, 120

Chen, C. H. K., Matteini, L., Schekochihin, A. A., et al. 2016, *ApJ*, 825, L26

Foot, E. A., & Kulsrud, R. M. 1979, *ApJ*, 233, 302

Fried, B. D., & Conte, S. D. 1961, *The Plasma Dispersion Function* (New York: Academic Press)

Gary, S. P. 1993, *Theory of Space Plasma Microinstabilities* (New York: Cambridge Univ. Press)

Ghosh, S., Matthaeus, W. H., Roberts, D. A., & Goldstein, M. L. 1998, *J. Geophys. Res.*, 103, 23705

Hellinger, P., Trávníček, P., Kasper, J. C., & Lazarus, A. J. 2006, *Geophys. Res. Lett.*, 33, 9101

Howes, G. G., Bale, S. D., Klein, K. G., et al. 2012, *ApJ*, 753, L19

Howes, G. G., Cowley, S. C., Dorland, W., et al. 2006, *ApJ*, 651, 590

Howes, G. G., Klein, K. G., & TenBarge, J. M. 2014, *ArXiv e-prints*, arXiv:1404.2913

Kasper, J. C. 2002, PhD thesis, Massachusetts Institute of Technology

Kasper, J. C., Lazarus, A. J., & Gary, S. P. 2002, *Geophys. Res. Lett.*, 29, 20

—. 2008, *Physical Review Letters*, 101, 261103

Kellogg, P. J., & Horbury, T. S. 2005, *Ann. Geophys.*, 23, 3765

Klein, K. G. 2013, PhD thesis, The University of Iowa, doi:10.5281/zenodo.50471

Klein, K. G., Howes, G. G., TenBarge, J. M., et al. 2012, *ApJ*, 755, 159

Kunz, M. W., Schekochihin, A. A., Chen, C. H. K., Abel, I. G., & Cowley, S. C. 2015, *Journal of Plasma Physics*, 81, 325810501

Kunz, M. W., Stone, J. M., & Quataert, E. 2016, *Phys. Rev. Lett.*, 117, 235101

Lepping, R. P., Acuña, M. H., Burlaga, L. F., et al. 1995, *Space Sci. Rev.*, 71, 207

Lin, R. P., Anderson, K. A., Ashford, S., et al. 1995, *Space Sci. Rev.*, 71, 125

Marsch, E., Schwenn, R., Rosenbauer, H., et al. 1982, *J. Geophys. Res.*, 87, 52

Marsch, E., & Tu, C. Y. 1993, *Ann. Geophys.*, 11, 659

McComas, D. J., Barraclough, B. L., Gosling, J. T., et al. 1995, *J. Geophys. Res.*, 100, 19893

Narita, Y., & Marsch, E. 2015, *ApJ*, 805, 24

Reisenfeld, D. B., McComas, D. J., & Steinberg, J. T. 1999, *Geophys. Res. Lett.*, 26, 1805

Riquelme, M. A., Quataert, E., & Verscharen, D. 2015, *ApJ*, 800, 27

—. 2016, *ApJ*, 824, 123

Salem, C. S., Howes, G. G., Sundkvist, D., et al. 2012, *ApJ*, 745, L9

Schekochihin, A. A., Cowley, S. C., Dorland, W., et al. 2009, *ApJS*, 182, 310

Schekochihin, A. A., Parker, J. T., Highcock, E. G., et al. 2016, *J. Plasma Phys.*, 82, 905820212

Stix, T. H. 1992, *Waves in plasmas* (New York: AIP)

Torrence, C., & Compo, G. P. 1998, *Bull. Am. Meteorol. Soc.*, 79, 61

Tu, C.-Y., & Marsch, E. 1994, *J. Geophys. Res.*, 99, 21

—. 1995, *Space Sci. Rev.*, 73, 1

Vellante, M., & Lazarus, A. J. 1987, *J. Geophys. Res.*, 92, 9893

Verscharen, D., Bourouaine, S., Chandran, B. D. G., & Maruca, B. A. 2013, *ApJ*, 773, 8

Verscharen, D., Chandran, B. D. G., Klein, K. G., & Quataert, E. 2016, *ApJ*, 831, 128

Verscharen, D., Marsch, E., Motschmann, U., & Müller, J. 2012, *Physics of Plasmas*, 19, 022305

Yang, L., He, J., Tu, C., et al. 2017, *ApJ*, 836, 69

Yao, S., He, J.-S., Marsch, E., et al. 2011, *ApJ*, 728, 146

Yao, S., He, J.-S., Tu, C.-Y., Wang, L.-H., & Marsch, E. 2013a, *ApJ*, 776, 94

—. 2013b, *ApJ*, 774, 59

Yoon, P. H. 2016, *ApJ*, 833, 106

Zank, G. P., & Matthaeus, W. H. 1993, *Phys. Fluids*, 5, 257

Zank, G. P., Matthaeus, W. H., & Klein, L. W. 1990, *Geophys. Res. Lett.*, 17, 1239